An Optimization-Driven Approach for Computing Geodesic Paths on Triangle Meshes

Bangquan Liu[a,b], Shuangmin Chen[a,*], Shi-Qing Xin[c], Ying He[d], Zhen Liu[a], Jieyu Zhao[a]

[a] *Faculty of Electrical Engineering and Computer Science, Ningbo University*
[b] *College of Information Engineering, Ningbo Dahongying University*
[c] *School of Computer Science and Technology, Shandong University*
[d] *School of Computer Engineering, Nanyang Technological University*

Abstract

There are many application scenarios where we need to refine an initial path lying on a surface to be as short as possible. A typical way to solve this problem is to iteratively shorten one segment of the path at a time. As local approaches, they are conceptually simple and easy to implement, but they converge slowly and have poor performance on large scale models. In this paper, we develop an optimization driven approach to improve the performance of computing geodesic paths. We formulate the objective function as the total length and adopt the L-BFGS solver to minimize it. Computational results show that our method converges with super-linear rate, which significantly outperforms the existing methods. Moreover, our method is flexible to handle anisotropic metric, non-uniform density function, as well as additional user-specified constraints, such as coplanar geodesics and equally-spaced geodesic helical curves, which are challenging to the existing local methods.

Keywords:
geodesic paths, geodesic helical curves, optimization, anisotropic metric, non-uniform density

1. Introduction

Computing geodesic distances and paths is a fundamental problem in computational geometry, and it plays an important role in a wide range of applications, including sampling [1], non-rigid registration [2], surface classification [3], geodesic Voronoi diagram [4, 5, 6], intrinsic Delaunay triangulation [7], shape segmentation [8, 9], texture mapping [10], parameterization [11, 12], image segmentation [13], and many others. Since polygonal meshes are the dominant shape representation scheme in computer graphics, solving the *discrete* geodesic problem [14] draws much attention, where the goal is to find the shortest path between two arbitrary points on a polyhedral surface. For many applications, the underlying mesh may be also associated with non-uniform density, anisotropic metric and user-specified geometric constraints.

There are two major classes of algorithms for computing discrete geodesic paths. Starting from the source point, the *global* methods propagate *discrete* wavefront across the faces in a Dijkstra-like sweep until reaching the destination. Representative works are the fast marching method [15], the Mitchell-Mount-Papadimitriou (MMP) algorithm [16], the Chen-Han (CH) algorithm [17] and their many variants [18, 19, 20, 21, 22, 23]. The global methods are able to find the *globally* shortest path, however they are computationally expensive. The *local* methods [24, 25, 26], on the other hand, adopt a completely different strategy. Starting from a given initial path connecting the two endpoints, they iteratively shorten the path until it becomes a locally shortest geodesic. The local methods are easy to implement, but they converge slowly and can find only the local optimal solution. It is worth noting that both the existing global and local methods are designed for meshes with Euclidean metrics only, so they are not able to handle meshes with anisotropic metric and user-specified density function and/or constraints.

In this paper, we propose an optimization-driven approach to tackle the above-mentioned challenges. We formulate the objective function using the total path length in terms of the intersection points on the edge sequence containing the path, so that anisotropic metric, density function and constraints are naturally supported. Thanks to the closed-form formula of its gradient, we are able to adopt the L-BFGS solver [27] to minimize the objective function, leading to empirically super-linear convergence rate. Our method works for both open and closed geodesic paths, and it is numerically stable so that the results are insensitive to mesh tessellation and resolution. We demonstrate its efficacy on meshes with anisotropic metric, non-uniform density and user-specified constraints, such as coplanar geodesics and equally-spaced geodesic helical curves. To our knowledge, our method is the first one with all these features.

The remaining of the paper is organized as follows: Section 2 reviews the related works on discrete geodesics, followed by background knowledge in Section 3. Then Section 4 documents our method in details and Section 5 reports the experimental results and showcases a few applications. Finally, Section 6 concludes the paper and points out future directions.

*Corresponding author: chenshuangmin@nbu.edu.cn (S. Chen).

2. Related Work

There is a large body of literature on the discrete geodesic problem. Due to space limit, we review only the most relevant work on computing geodesic paths.

Global Wavefront Propagation Methods. This type of methods is often used to compute a distance field rooted at a given source point or a globally shortest path between two given points. Most of them (e.g., [28, 16, 17, 15, 18, 29, 20, 21, 22, 23]) adopt Dijkstra's framework to propagate discrete wavefronts. Due to the global nature, these methods are able to find the globally shortest path, but at a high computational cost. Moreover, these methods are designed for meshes with Euclidean metrics only, and it is difficult to extend them for meshes with non-uniform density function and/or anisotropic metric.

PDE Methods. Crane et al. [30] proposed a heat equation based method that initializes the source point with a unit of heat, diffuses it in a very short time and finally rebuilds the geodesic distance field using the gradients of the heat field. The heat method enables information reuse and outperforms the discrete wavefront propagation methods in terms of performance. It also works for point clouds and meshes with anisotropic metric [31]. However, it computes only approximate solutions which are highly sensitive to mesh triangulation and resolution. Solomon et al. [32] showed that the earth mover's distance (EMD) between two delta distributions reduces to geodesic distance. Their method is able to compute a family of distances ranging from geodesic distance to bi-harmonic distance [33]. However, the high computational cost diminishes its applications to large-scale models. It is also not clear whether the PDE approaches can solve constrained geodesic problems.

Graph-based Methods. Graph-based methods solve the discrete geodesic problem by constructing an undirected graph G so that a geodesic path on the mesh M is (approximately) equal to a shortest path on G. Aleksandrov et al. [34] suggested adding a logarithmic number of Steiner points along each edge of the mesh, which are placed in a geometric progression along an edge. Then it takes $O(mn\log(mn) + nm^2)$ time to compute a $(1+\varepsilon)$-approximation geodesic path, where m is the total number of Steiner points. Xin et al. [35] adopted a different strategy by adding m (specified by the user) uniformly distributed auxiliary points on the mesh. Then they constructed a graph with $O(m^2+n)$ edges in $O(mn^2\log n)$ time. Such a graph enables computing geodesic distance between any pair of points (unnecessarily mesh vertices) in constant time $O(1)$. However, the price to pay is the quadratic space complexity of the *dense* graph, resulting poor scalability. Both saddle vertex graph and discrete geodesic graph are *sparse* graphs. Observing that most geodesic paths on real-world meshes can be partitioned into shorter segments by saddle vertices, Ying et al. [36] proposed the saddle vertex graph (SVG) to compute geodesic distances in a divide-and-conquer manner. Recently, Wang et al. [37] developed discrete geodesic graph, which enables direct error control.

Local and Iterative Methods. There are many applications where one already has an initial path and intends to refine it to a geodesic at a little computational cost. A typical technique is to iteratively shorten the path by local perturbation like shrinking a rubber band [24, 25, 26]. These approaches are easy to implement, however they have only linear convergence rate, and their performance is highly sensitive to initialization. In this paper, we propose a better iterative scheme with an explicit objective function whose gradient can be evaluated in closed-form formula. This allows us to adopt the efficient L-BFGS solver to minimize the function. This seemingly minor change brings at least two benefits. On one hand, it significantly improves the performance due to its superlinear convergence rate. On the other hand, the new algorithm is purely optimization driven, hereby it naturally supports anisotropic metric, user-specified density function and constraints.

3. Preliminary

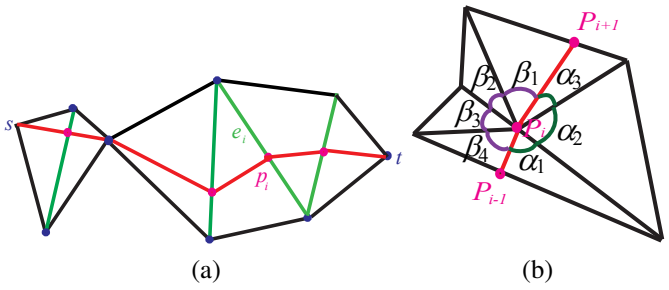

Figure 1: (a) A discrete path can be encoded using the face sequence containing it. (b) A path (P_{i-1}, P_i, P_{i+1}) passes through vertex P_i and it splits the cone angle at P_i into two parts. To be an *exact* geodesic path, both angles $\sum_{i=1}^{3}\alpha_i$ and $\sum_{j=1}^{4}\beta_j$ are greater than or equal to π. In contrast, our algorithm computes an *approximate* geodesic path by relaxing such a constraint.

Denote by $M = (V, E, F)$ a connected, manifold triangle mesh, where V, E, F are the vertex, edge and face sets respectively. A vertex is called spherical, Euclidean or saddle if its cone angle is less than, equal to, or greater than 2π. Given two points $p, q \in M$, the geodesic path between p and q is denoted by $\gamma(p,q)$. Since geodesic paths are not unique in general, unless otherwise specified, $\gamma(p,q)$ refers to the global shortest geodesic path in this paper. Mitchell et al. [16] showed that a geodesic path on a mesh is an alternating sequence of vertices and (possibly empty) edge sequences such that the unfolded image of the path along any edge sequence is a straight line segment and the angle of γ passing through a vertex is greater than or equal to π, as shown in Figure 1(a).

The existing local geodesic methods [25, 24, 26, 38] are mainly designed based on this property. They generally require two common operations, shortening the path and updating the edge sequence containing it. Commonly used path shortening techniques are graph refinement [25], Laplacian smoothing [24] and edge sequence unfolding [26, 38], in which the angle checking rule is strictly enforced at each iteration, i.e., both of the angles split by the path are greater than or equal to π. However, they lack a clear objective function defined on

the whole path, which is crucial to optimization. When the base mesh is equipped with anisotropic metric and non-uniform density function or user-specified geometric constraints, the desirable path does not follow the angle checking rule and therefore the existing local methods cannot deal with these complicated cases. This motivates us to develop an optimization driven approach to refine the intimal path without any angle checking operations.

4. Algorithm

4.1. Formulation

Let $\mathcal{S}$ be a triangulated polyhedral surface in $\mathcal{R}^3$, defined by a set of vertices, edges, and faces. Given two points $s, t \in \mathcal{S}$, there are infinitely many paths between them. Our task is to refine an initial path to an as-short-as-possible path that meets given requirements. Let's assume the base mesh have a uniform density and identity metric at this moment. We will extend the algorithmic framework to non-uniform density setting and anisotropic metric in Section 4.3.

As Figure 1 shows, the initial path (shown in red) through the face sequence Γ can be described by $(s, p_1, p_2, \cdots, p_k, t)$, where p_i is the intersection point between the path and the i-th edge $e_i \triangleq (v_{e_i}^{(1)}, v_{e_i}^{(2)})$ in the face sequence. Then p_i can be represented by a scalar $\lambda_i \in [0, 1]$ so that $p_i = (1-\lambda_i)v_{e_i}^{(1)} + \lambda_i v_{e_i}^{(2)}$. The total path length is

$$L(\Gamma; \lambda_1, \lambda_2, \cdots, \lambda_k) = \|\overrightarrow{sp_1}\| + \sum_{i=1}^{k-1} \|\overrightarrow{p_i p_{i+1}}\| + \|\overrightarrow{p_k t}\|. \quad (1)$$

It is easy to compute the partial derivatives

$$\frac{\partial L}{\partial \lambda_i} = \begin{cases} (v_1^{(2)} - v_1^{(1)}, \frac{\overrightarrow{sp_1}}{\|\overrightarrow{sp_1}\|} - \frac{\overrightarrow{p_1 p_2}}{\|\overrightarrow{p_1 p_2}\|}), i = 1, \\ (v_i^{(2)} - v_i^{(1)}, \frac{\overrightarrow{p_{i-1} p_i}}{\|\overrightarrow{p_{i-1} p_i}\|} - \frac{\overrightarrow{p_i p_{i+1}}}{\|\overrightarrow{p_i p_{i+1}}\|}), 1 < i < k, \\ (v_k^{(2)} - v_k^{(1)}, \frac{\overrightarrow{p_{k-1} p_k}}{\|\overrightarrow{p_{k-1} p_k}\|} - \frac{\overrightarrow{p_k t}}{\|\overrightarrow{p_k t}\|}), i = k. \end{cases} \quad (2)$$

Suppose that the user-specified constraints can be represented by $H(\Gamma; \lambda_1, \lambda_2, \cdots, \lambda_k) = 0$. To this end, our task is to find a face sequence Γ, as well as a collection of numbers $\lambda_1, \lambda_2, \cdots, \lambda_k$, so as to

$$\text{minimize} \quad L(\Gamma; \lambda_1, \lambda_2, \cdots, \lambda_k) + M \times H^2(\Gamma; \lambda_1, \lambda_2, \cdots, \lambda_k)$$

subject to

$$0 \le \lambda_i \le 1, 1 \le i \le k,$$

where M is a sufficiently large coefficient. In general, a large penalty parameter M leads to solutions satisfying the constraint, but it often increases the fluctuation of the objective function. In our setting, we empirically set M so that the penalty term is about 10 times the total length.

4.2. Implementation

Different from general optimization problems, the as-short-as-possible path problem needs to update the face sequence in the optimization process. Our basic idea is that during each iteration we perform the following operations: (1) compute the value and the gradients of $L + M \times H^2$, (2) update $\lambda_1, \lambda_2, \cdots, \lambda_k$ according to the direction and the step size recommended by L-BFGS, (3) pull each λ_i to $[0, 1]$, and (4) update the current face sequence where $\lambda_i = 0$ or $\lambda_i = 1$.

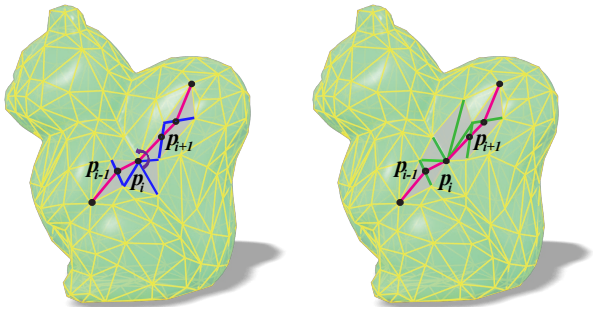

(a) (b)

Figure 3: If the current path passes through one of the vertices, say, p_i, then we update the face sequence from (a) to (b).

We use Figure 2 to demonstrate a refining process on a 2D mesh. It can be seen from the plots of path length and its gradient norm that our algorithm has a desirable convergence rate and greatly outperforms the existing iterative algorithm proposed by [24]; See the length and gradient-norm decreasing plots in this figure. We will evaluate its performance in detail in the next section. The pseudo-code is shown in Algorithm 1.

As one of the key routines, we have to update the face sequence when λ_i reaches 0 or 1. Taking Figure 3 as an example, the current path pass through p_i that is a mesh vertex. p_i is on the left side of the current triangle strip (whose boundary consists of two sequences of vertices). We traverse the face sequence from beginning to end and change the face sequence such that p_i is on the right side of the new face sequence.

Input: A triangle Mesh $\mathcal{S}$; two points $s, t \in \mathcal{S}$ and an initial path between them; A error tolerance ϵ.
Output: A geodesic path between s and t.
while *the length difference between two successive iterations is larger than* ϵ **do**
  Compute the length of $L(\Gamma) + M \times H^2(\Gamma)$;
  Compute the gradient $\nabla(L(\Gamma) + M \times H^2(\Gamma))$;
  Get the resulting path;
  Collect the vertices $\{v_i\}$ on the path;
  Traverse and update the face sequence such that each $v \in \{v_i\}$ is on the other side of the new face sequence.
end

Algorithm 1: A optimization based method for computing an as-short-as-possible path.

Remark: Our algorithm has two differences from the conventional iterative scheme. First, the conventional iterative algorithm does not update face sequence until the path constrained on the current face sequence has been found, while our algorithm performs face sequence updating when $\lambda_i = 0$ or $\lambda_i = 1$. Second, when updating the face sequence, the conventional iterative algorithm needs to check the angles passing through each

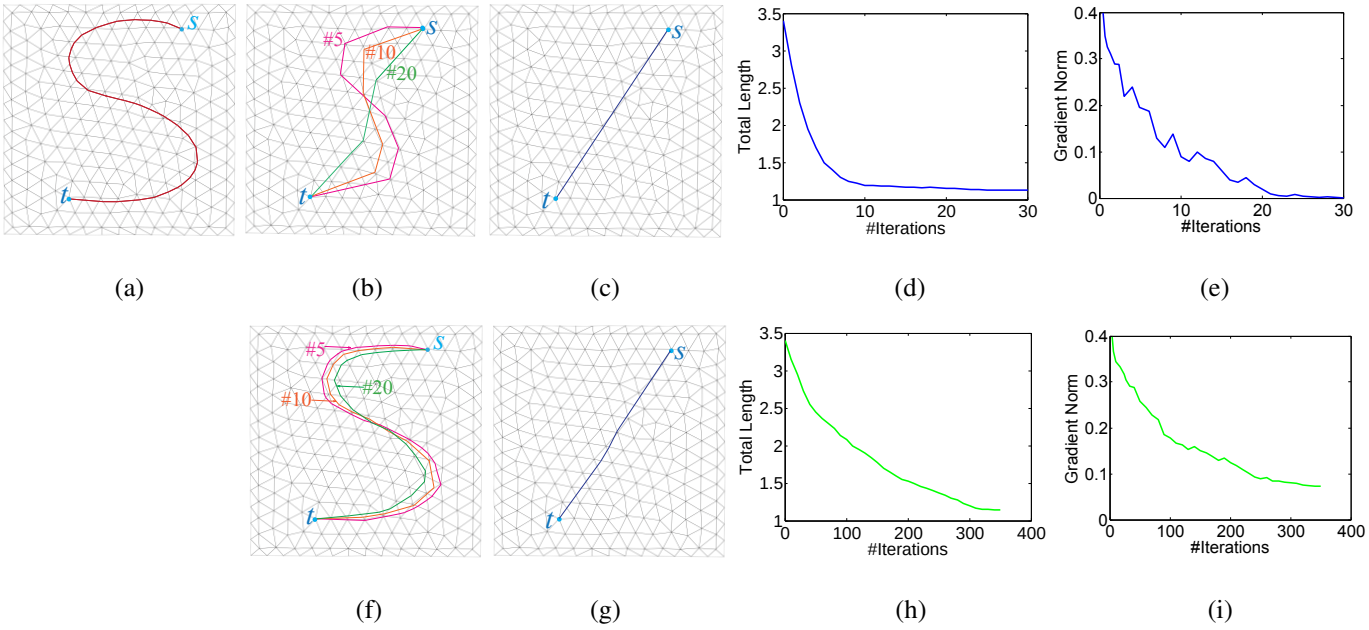

Figure 2: An example on a 2D mesh. (a) shows the initial path. (b) Three intermediate results for iteration 5, 10, and 20. (c) Our algorithm terminates after 30 iterations, with the gradient norm less than 10^{-6}. The resulting path has a relative error less than 10^{-6}. (d) and (e) show the plots of objective function and its gradient norm. (f) shows three intermediate results of Martínez et al.'s algorithm [24]. (g) After 350 iterations, their algorithm produces the path with relative error 0.3%. As shown in (h) and (i), their algorithm has rather low convergence rate comparing to ours.

vertex to guarantee that at the conclusion of the algorithm, the angles on both sides are greater than or equal to π, as Figure 1(b) shows. However, our goal is to find an as-short-as-possible path and thus our algorithm does not include such a step of angle checking.

4.3. *Meshes with Non-Uniform Density and/or Anisotropic Metric*

First, we will discuss the case where the base mesh has a non-uniform density function defined on the surface. Typically, each polygonal face f_i has a constant density value $\rho(f_i)$. In this case, the total path length is given by

$$L(\Gamma;\lambda_1,\lambda_2,\cdots,\lambda_k) = \rho(\overrightarrow{sp_1})\|\overrightarrow{sp_1}\| + \sum_{i=1}^{k-1}\rho(\overrightarrow{p_ip_{i+1}})\|\overrightarrow{p_ip_{i+1}}\| + \rho(\overrightarrow{p_kt})\|\overrightarrow{p_kt}\|, \tag{3}$$

whose gradient with regard to λ_i is

$$\frac{\partial L}{\partial \lambda_i} = \begin{cases} (v_1^{(2)} - v_1^{(1)}, \rho(\overrightarrow{sp_1})\frac{\overrightarrow{sp_1}}{\|\overrightarrow{sp_1}\|} - \rho(\overrightarrow{p_1p_2})\frac{\overrightarrow{p_1p_2}}{\|\overrightarrow{p_1p_2}\|}), & i = 1 \\ (v_i^{(2)} - v_i^{(1)}, \rho(\overrightarrow{p_{i-1}p_i})\frac{\overrightarrow{p_{i-1}p_i}}{\|\overrightarrow{p_{i-1}p_i}\|} - \rho(\overrightarrow{p_ip_{i+1}})\frac{\overrightarrow{p_ip_{i+1}}}{\|\overrightarrow{p_ip_{i+1}}\|}), & 1 < i < k \\ (v_k^{(2)} - v_k^{(1)}, \rho(\overrightarrow{p_{k-1}p_k})\frac{\overrightarrow{p_{k-1}p_k}}{\|\overrightarrow{p_{k-1}p_k}\|} - \rho(\overrightarrow{p_kt})\frac{\overrightarrow{p_kt}}{\|\overrightarrow{p_kt}\|}), & i = k, \end{cases} \tag{4}$$

where $\rho(\overrightarrow{AB})$ denotes the density in the face containing the line segment $\overrightarrow{AB}$. It's easy to know that if the density is uniform on the surface, then the above formulation degenerates into Eq. (1) and Eq. (2). Otherwise, the path tends to go through the area with a low density. As Figure 4 shows, we locally set a Gaussian density function to Bimba (400K faces), Horse (40K faces) and Buddha (600K faces) respectively to see how the density setting influences the geodesic paths. It can seen that the density-weighted geodesics (shown in blue) tend to pass through the area with low density.

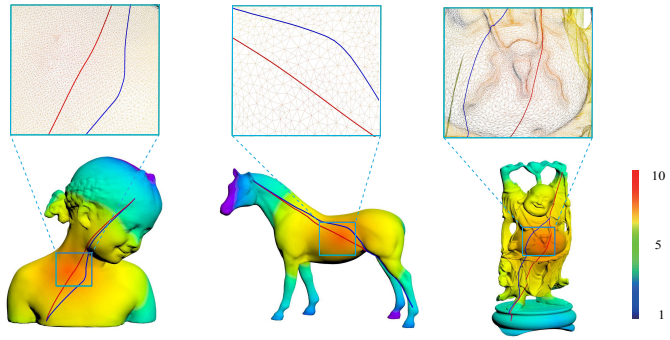

(a) Bimba (b) Horse (C) Buddha

Figure 4: We locally set a Gaussian density function to Bimba, Horse and Buddha respectively and observe how the density setting influences the geodesic paths. The red paths are geodesics assuming the density is uniform on the surface, while the blue paths are geodesics in the non-uniform density setting.

When the input mesh carries an anisotropic metric, we can assume that each face is associated with two orthogonal vectors $(\vec{\tau}_1, \vec{\tau}_2)$ in the discrete setting. In real computation, we assign each face with a 2×2 matrix to denote the anisotropic metric operator. Let $T(f_i)$ be the matrix on the face f_i. The total path length is given by

$$L(\lambda_1,\lambda_2,\cdots,\lambda_k) = \|T(\overrightarrow{sp_1})\| + \sum_{i=1}^{k-1}\|T(\overrightarrow{p_ip_{i+1}})\| + \|T(\overrightarrow{p_kt})\|, \tag{5}$$

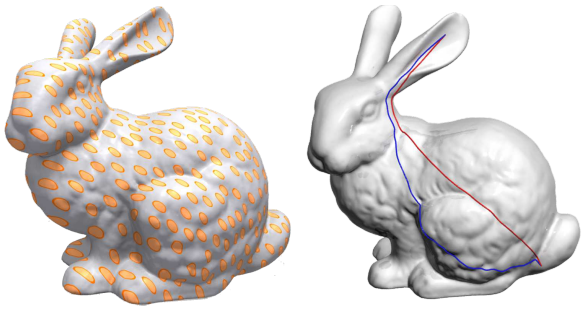

(a) (b)

Figure 5: Anisotropic/Isotropic geodesic paths. The red path in (b) is a geodesic under the isotropic and uniform metric, while the blue path is computed under the anisotropic metric shown in (a).

whose gradient with regard to λ_i is

$$\frac{\partial L}{\partial \lambda_i} = \begin{cases} (v_1^{(2)} - v_1^{(1)}, \frac{T(\overrightarrow{sp_1})}{\|T(\overrightarrow{sp_1})\|} - \frac{T(\overrightarrow{p_1p_2})}{\|T(\overrightarrow{p_1p_2})\|}), & i = 1 \\ (v_i^{(2)} - v_i^{(1)}, \frac{T(\overrightarrow{p_{i-1}p_i})}{\|T(\overrightarrow{p_{i-1}p_i})\|} - \frac{T(\overrightarrow{p_ip_{i+1}})}{\|T(\overrightarrow{p_ip_{i+1}})\|}), & 1 < i < k \\ (v_k^{(2)} - v_k^{(1)}, \frac{T(\overrightarrow{p_{k-1}p_k})}{\|T(\overrightarrow{p_{k-1}p_k})\|} - \frac{T(\overrightarrow{p_kt})}{\|T(\overrightarrow{p_kt})\|}), & i = k \end{cases} \quad (6)$$

where $T(\overrightarrow{AB})$ denotes the 2×2 matrix encoding the anisotropic metric in the face containing the line segment $\overrightarrow{AB}$. As Figure 5 shows, the left-side figure shows the anisotropic metric on the surface, while the right-side figure shows two geodesics under the isotropic/anisotropic metrics. To sum up, even if the base mesh has a non-uniform density setting or an anisotropic metric, we can still use the same optimization based algorithmic framework to compute the as-short-as-possible path that meets the user-specified constraints.

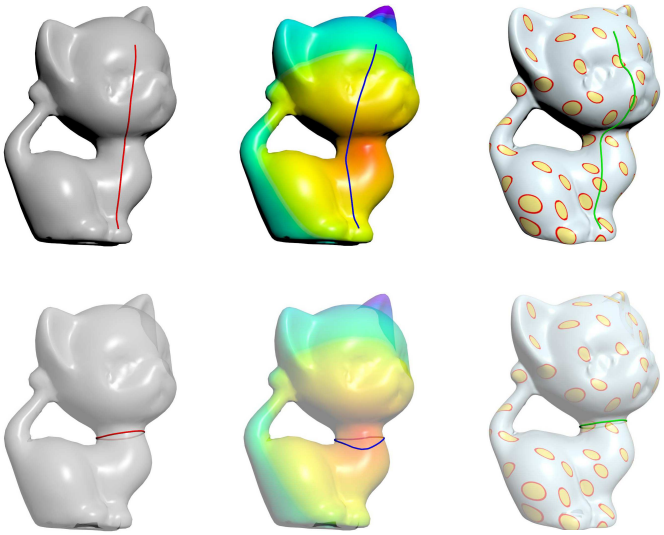

Figure 6: Computing open/closed geodesic using our algorithm. The model in the left column adopts isotropic metric, whereas the middle and right columns show the models with non-uniform density and anisotropic metric respectively.

5. Results & Applications

We implemented our algorithm in C++ and OpenMP, and conducted the experiments on a PC with a 3.07GHz Intel(R) Core(TM) i7 CPU and 6 GB memory.

5.1. Qualitative Comparison

First, we evaluated its performance and compared it to five representative methods:

- The geodesic algorithm in this paper, where the initial path is given by FMM [15];
- The fast marching method (FMM) [15];
- The improved fast marching method (IFMM) [26];
- The iterative method by Martínez et al. [24], where the initial path is given by FMM [15].
- The improved Chen & Han's (ICH) algorithm [20];
- The fast wavefront propagation (FWP) geodesic algorithm [22].

In Table 1, we show qualitative comparison of the above-mentioned five representative methods. In Figure 6, we show some examples of open/closed geodesics on the Kitten model, where the left column doesn't assume any density setting or anistropic metric, the middle column assumes a non-uniform density function, the right column assumes an anistropic metric setting. To summarize, our algorithm is able to compute open/closed geodesics, handle non-uniform density setting and anistropic metrics, and support additional geometric constraints. These merits distinguish our algorithm from the existing geodesic approaches.

It's worth noting that the iterative method by Martínez et al. [24] cannot support non-uniform density setting or anisotropic metric since it has to perform an angle checking step as Figure 1(b) shows.

5.2. Quantitative Comparison

Now let's assume that the input doesn't have non-uniform density or anisotropic metric and observe the performance contrast. For comparison purpose, we set the termination condition to be $|L - L^*|/L^* < 0.1\%$, where L^* is the exact geodesic distance. At the same time, we randomly sample 10K pairs of vertices to take down the average computation time.

We use the Bunny model as the test model, which is meshed into various resolutions ranging from $20K$ to $100K$ faces. Table 2 shows the timing statistics, from which we can clearly see an performance advantage compared with the existing algorithms, whether local scheme [24] or global ones [20, 15]. See Figure 7(a). We must point out that the approach by Martínez et al. [24] only has linear convergence rate since it is not guided by gradients. Our algorithm takes advantage of gradients and benefits from the L-BFGS solver. For the Bunny model with $100K$ faces, our algorithm takes 1.15 seconds averagely to compute a geodesic path while the iterative algorithm in [24] requires

Table 1: Features of geodesic algorithms

Method	Open geodesic	Geodesic loop	Density function	Anisotropy metric	Geometric constraints
Ours	✓	✓	✓	✓	✓
FMM	✓	×	✓	✓	×
IFMM	✓	×	×	×	×
ICH	✓	×	×	×	×
FWP	✓	×	×	×	×
Martínez et al.	✓	✓	×	×	×

Table 2: Performance of representative algorithms on the Bunny model in various resolutions

#Faces	Ours		IFMM [26]		Our+IFMM		Xin-Wang [20]		FWP [22]		Martínez et al. [24]	
	Time (s)	$\lvert L-L^*\rvert/L^*$	Time (s)	$\lvert L-L^*\rvert/L^*$	Time (s)	$\lvert L-L^*\rvert/L^*$	Time (s)	$\lvert L-L^*\rvert/L^*$	Time (s)	$\lvert L-L^*\rvert/L^*$	Time (s)	$\lvert L-L^*\rvert/L^*$
20K	0.18	0.001	0.23	1.217	0.41	0.001	0.65	–	0.35	–	10.29	0.001
40K	0.25		0.43	0.958	0.68		1.93		0.62		18.48	
60K	0.38		0.75	0.786	1.13		4.17		1.78		34.46	
80K	0.65		1.04	0.518	1.69		7.24		2.89		56.63	
100K	0.98		1.63	0.485	2.66		14.11		5.16		83.53	
150K	1.89		3.15	0.366	5.04		23.87		8.04		108.86	
200K	3.21		6.56	0.187	9.77		37.11		14.61		160.34	
300K	4.96		11.12	0.089	16.08		58.89		21.78		246.65	

85 seconds in average. We show the length decreasing plots in Figure 7(b). The significant contrast shows that our algorithm has super-linear convergence rate. It's worth noting that their iterative algorithm converges very slowly especially when the path is close to the exact geodesic. In spite of this, we must point out that both of them depends on initialization and may converge into a geodesic path that is different from the globally shortest path.

5.3. Applications

In this section, we shall exhibit its uses to three typical application occasions including (1) closed geodesics, (2) coplanar geodesics on surfaces and (3) equally-spaced geodesic helix curves.

5.3.1. Geodesic Loops

Geodesic loops [38, 39], or closed geodesic curves, are useful in mesh cutting, girth estimation, and topology analysis. A closed curve is said to be a geodesic loop if every subpath is an open geodesic. Note that for most problems, "stable" geodesic loops robust to small perturbance are of our interest. Xin et al. [38] proposed a shortening technique to compute geodesic loops but their method has to repeatedly unfold a long face sequence, which is a tedious and time-consuming step. Wu and Tai [39] suggested finding the level set where the geodesic curvature is zero. However, their method doesn't have a desirable performance according to their timing statistics. Obviously our algorithm can be naturally extended to compute geodesic loops without any modification as long as it is initialized by a closed curve, see in Figure 8. Compared with the existing methods, our algorithm has a better performance. For example, for the horse model with 20K faces, it only takes 0.19 seconds in average to compute a geodesic loop, which shows that our algorithm can be used to interactive mesh cutting. Besides, we must point

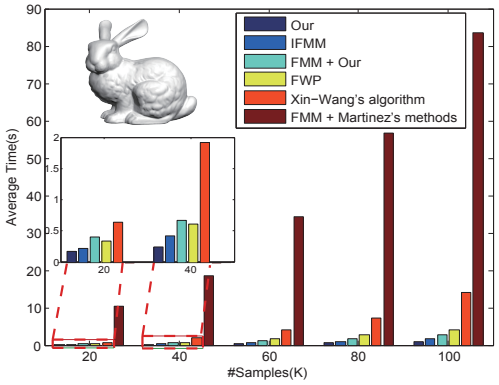

(a)

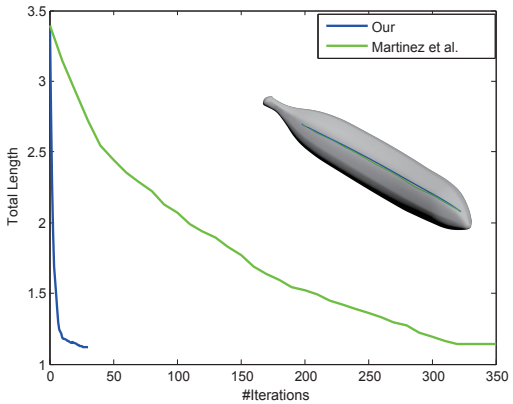

(b)

Figure 7: Performance comparison. Our algorithm has an performance advantage compared with the existing algorithms (a), which is due to the super-linear convergence rate (b). Note that the iterative approach [24] only has linear convergence rate since it is not guided by gradients.

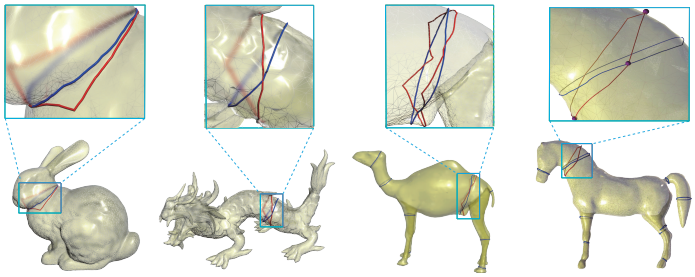

Figure 8: Our algorithm is able to compute geodesic loops.

out even if the base mesh has a background density function or anisotropic metric, our algorithm still works well, which is a desirable feature in many practical applications.

5.3.2. *Co-Planar Geodesics*

In the computer graphic community, there are many problems that need to find an as-short-as-possible path that meet the user-specified constraints. For example, given an initial open/closed curve, can we find a coplanar curve that is as short as possible? That is to say, we need to minimize the total length

$$L(\lambda_1, \lambda_2, \cdots, \lambda_k) = \|\overrightarrow{sp_1}\| + \sum_{i=1}^{k-1} \|\overrightarrow{p_i p_{i+1}}\| + \|\overrightarrow{p_k t}\|, \tag{7}$$

subject to

$$\begin{cases} \overrightarrow{n} \cdot p_1 - d = 0, \\ \overrightarrow{n} \cdot p_2 - d = 0, \\ \quad \vdots \\ \overrightarrow{n} \cdot p_k - d = 0. \end{cases} \tag{8}$$

where d is the signed distance from the origin to the plane, k is the number of geodesic points, and $\overrightarrow{n}$ is the plane normal. Figure 9 gave a group of examples on co-planar geodesics.

(a) (b) (c)

Figure 9: Coplanar geodesics. In (a), (b) and (c), the blue paths are the resulting coplanar geodesics refined from the initial red paths.

5.3.3. *Geodesic Helix Curves*

Another example is the geodesic winding problem [40, 41], where a family of equally spaced geodesic curves needs to be spread out on the surface of an input 3D object, which is very useful in the manufacturing field. However, it's highly non-trivial to guarantee that the geodesic curves are uniformly distributed on the surface. Xin et al. [41] pointed out that a geodesic helix curve tends to pass through the narrow area. Therefore, we want to find a special density setting such that the curve length gets punished when passing through the narrow area. We observe that such a density setting is desirable: for each point p on the surface, we set the density $\rho(p)$ to be in inverse proportion to its "girth", denoted by $g(p)$, that is defined to be the length of the shortest p-constrained geodesic loop [42]. Mathematically, the weighted path length is

$$L = \int_0^1 \frac{1}{g(p)} \mathrm{d}s.$$

In implementation, we use the method proposed in [42] to precompute the girth function, and then generate an N-winding initial path on the surface. Finally we use the algorithm in this paper to refine it to be a geodesic. It's worth noting that Xin et al.'s algorithm [41] does not support user-specified density function, hereby their result is far from being equally spaced. In sharp contrast, our algorithm can naturally deal with non-uniform density function, and produce equally spaced helical curve. See Figure 10.

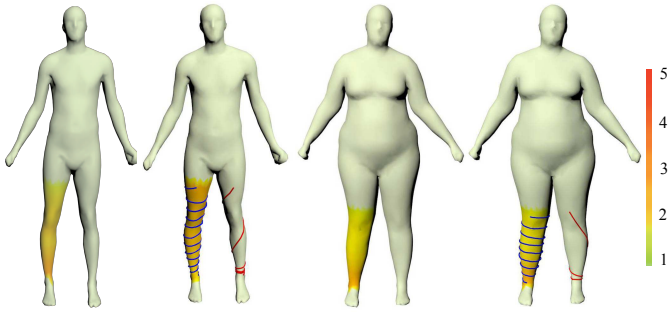

(a) (b) (c) (d)

Figure 10: Equally spaced geodesic helical curves on synthetic and real-world models. The density functions (a) and (c) are visualized using color map, where the warm and cold colors denote high and low densities respectively. In (b) and (d), the red curves are the quasi-helixes computed by Xin et al. [41] . while the blue curves are computed by our algorithm.

6. Conclusions and Future Works

In this paper, we propose an optimization based approach that is different from conventional algorithmic schemes. The distinguished feature of the new algorithmic framework is that it supports non-uniform density setting, anisotropy metric and additional geometric constraints at the same time. For example, the new algorithm enables us to compute co-planar geodesics or equally-spaced geodesic helix curves. Equipped with an L-BFGS solver, our algorithm exhibits a high computational performance. We believe that it has a great potential for many computer graphics occasions especially when one wants to find an as-short-as-possible path while meeting some specific geometric requirements. In the future, we will keep improving the performance by advanced parallelization techniques. We will also explore more applications in visual computing.

Acknowledgement

We are grateful to the editors and anonymous reviewers for their insightful comments and suggestions. The models in

this paper are provided courtesy of the AIM @SHAPE Shape Repository. This work is partially supported by K.C. Wong Magna Fund in Ningbo University, NSF of China (61571247, 61373068, U1636111), NSF of ZheJiang (LZ16F030001), NSF of Ningbo (2016A610041), the Opening Foundation of Zhejiang Provincial Top Key Discipline(xkxl1517), MOE2013-T2-2-011 and MOE RG23/15.

References

[1] Ying X, Xin SQ, Sun Q, He Y. An intrinsic algorithm for parallel poisson disk sampling on arbitrary surfaces. IEEE Transactions on Visualization & Computer Graphics 2013;19(9):1425–37.

[2] Huang Q, Bart A, Martin W, Guibas LJ. Non-rigid registration under isometric deformations. Computer Graphics Forum 2008;27(5):1449–57.

[3] Jin M. Computing geodesic spectra of surfaces. In: ACM Symposium on Solid and Physical Modeling. 2007, p. 387–93.

[4] Liu YJ, Chen Z, Tang K. Construction of iso-contours, bisectors, and Voronoi diagrams on triangulated surfaces. IEEE Transactions on Pattern Analysis & Machine Intelligence 2010;33(8):1502–17.

[5] Xu C, Liu Y, Sun Q, Li J, He Y. Polyline-sourced geodesic Voronoi diagrams on triangle meshes. Comput Graph Forum 2014;33(7):161–70.

[6] Liu Y, Xu C, Yi R, Fan D, He Y. Manifold differential evolution (MDE): a global optimization method for geodesic centroidal Voronoi tessellations on meshes. ACM Trans Graph 2016;35(6):243:1–243:10.

[7] Liu Y, Xu C, Fan D, He Y. Efficient construction and simplification of Delaunay meshes. ACM Trans Graph 2015;34(6):174:1–174:13.

[8] Troy F, Attali D. From a closed piecewise geodesic to a constriction on a closed triangulated surface. In: Pacific Conference on Computer Graphics and Applications. 2003, p. 394.

[9] Peyré G, Cohen L. Surface segmentation using geodesic centroidal tesselation. In: International Symposium on 3D Data Processing, Visualization and Transmission, 2004. 3dpvt 2004. Proceedings. 2004, p. 995–1002.

[10] Sun Q, Zhang L, Zhang M, Ying X, Xin S, Xia J, et al. Texture brush: an interactive surface texturing interface. In: Proceedings of ACM Symposium on Interactive 3D Graphics and Games, I3D '13. 2013, p. 153–60.

[11] Sander PV, Wood ZJ, Gortler SJ, Snyder J, Hoppe H. Multi-chart geometry images. In: Eurographics/ACM SIGGRAPH Symposium on Geometry Processing. 2003, p. 146–55.

[12] Zhou K, Synder J, Guo B, Shum HY. Iso-charts: stretch-driven mesh parameterization using spectral analysis. In: Eurographics/ACM SIGGRAPH Symposium on Geometry Processing. 2004, p. 45–54.

[13] Liu Y, Yu C, Yu M, He Y. Manifold SLIC: A fast method to compute content-sensitive superpixels. In: Proceedings of IEEE CVPR'16. 2016, p. 651–9.

[14] Mitchell JSB. Geometric shortest paths and network optimization handbook of computational geometry. Elsevier Science Publishers B V 2015;:49–119.

[15] Kimmel R, Sethian JA. Computing geodesic paths on manifolds. Proceedings of the National Academy of Sciences of the United States of America 1998;95(15):8431–5.

[16] Mitchell JSB, Mount DM, Papadimitriou CH. The discrete geodesic problem. SIAM J Comput 1987;16(4):647–68.

[17] Chen J, Han Y. Shortest paths on a polyhedron. In: Proceedings of the sixth annual symposium on Computational geometry. ACM; 1990, p. 360–9.

[18] Surazhsky V, Surazhsky T, Kirsanov D, Gortler SJ, Hoppe H. Fast exact and approximate geodesics on meshes. ACM Transactions on Graphics 2005;24(3):553–60.

[19] Weber O, Devir YS, Bronstein AM, Bronstein MM, Kimmel R. Parallel algorithms for approximation of distance maps on parametric surfaces. ACM Trans Graph 2008;27(4).

[20] Xin SQ, Wang GJ. Improving Chen and Han's algorithm on the discrete geodesic problem. ACM Transactions on Graphics 2009;28(4):104.

[21] Ying X, Xin SQ, He Y. Parallel Chen-Han (PCH) algorithm for discrete geodesics. ACM Transactions on Graphics 2014;33(1):57–76.

[22] Xu C, Wang TY, Liu Y, Liu L, He Y. Fast wavefront propagation (FWP) for computing exact geodesic distances on meshes. IEEE Trans Vis Comput Graph 2015;21(7):822–34.

[23] Qin Y, Han X, Yu H, Yu Y, Zhang J. Fast and exact discrete geodesic computation based on triangle-oriented wavefront propagation. ACM Transactions on Graphics 2016;35(4).

[24] Martínez D, Velho L, Carvalho PC. Computing geodesics on triangular meshes. Computers & Graphics 2005;29(5):667–75.

[25] Kanai T, Suzuki H. Approximate shortest path on a polyhedral surface based on selective refinement of the discrete graph and its applications. In: Geometric Modeling and Processing. 2000, p. 241–50.

[26] Xin SQ, Wang GJ. Efficiently determining a locally exact shortest path on polyhedral surfaces. Computer-Aided Design 2007;39(12):1081–90.

[27] Liu DC, Nocedal J. On the limited memory BFGS method for large scale optimization. Mathematical Programming 1989;45(3):503–28.

[28] Sharir M, Schorr A. On shortest paths in polyhedral spaces. SIAM J Comput 1986;15(1):193–215.

[29] Peyré G, Cohen LD. Heuristically driven front propagation for fast geodesic extraction. Lecture Notes in Computer Science 2008;3752(1):173–85.

[30] Crane K, Weischedel C, Wardetzky M. Geodesics in heat: A new approach to computing distance based on heat flow. ACM Transactions on Graphics 2013;32(5):152.

[31] Campen M, Heistermann M, Kobbelt L. Practical anisotropic geodesy. Comput Graph Forum 2013;32(5):63–71.

[32] Solomon J, Rustamov R, Guibas L, Butscher A. Earth mover's distances on discrete surfaces. ACM Trans Graph 2014;33(4):67:1–67:12.

[33] Lipman Y, Rustamov RM, Funkhouser TA. Biharmonic distance. ACM Transactions on Graphics 2010;29(3):483–96.

[34] Aleksandrov L, Lanthier M, Maheshwari A, Sack JR. An ε-approximation for weighted shortest paths on polyhedral surfaces. In: Proceedings of the 6th Scandinavian Workshop on Algorithm Theory (SWAT '98). 1998, p. 11–22.

[35] Xin SQ, Ying X, He Y. Constant-time all-pairs geodesic distance query on triangle meshes. In: Proceedings of the ACM SIGGRAPH Symposium on Interactive 3D Graphics and Games. 2012, p. 31–8.

[36] Ying X, Wang X, He Y. Saddle vertex graph (SVG): A novel solution to the discrete geodesic problem. ACM Transactions on Graphics 2013;32(6):170:1–12.

[37] Wang X, Fang Z, Wu J, Xin SQ, He Y. Discrete geodesic graph (DGG) for computing geodesic distances on polyhedral surfaces. Computer Aided Geometric Design 2017;52?3:262 –84.

[38] Xin SQ, He Y, Fu CW. Efficiently computing exact geodesic loops within finite steps. IEEE Transactions on Visualization and Computer Graphics 2012;18(6):879–89.

[39] Wu C, Tai X. A level set formulation of geodesic curvature flow on simplicial surfaces. IEEE Transactions on Visualization and Computer Graphics 2010;16(4):647–62.

[40] Mukhambetzhanov SG, Romashov YP, Sidorin SG, Tsentovskii EM. Geodesic winding on conical surfaces of arbitrary profile. Mechanics of Composite Materials 1993;28(6):540–5.

[41] Xin SQ, Chen S, Zhao J, Pan Z. Measuring length and girth of a tubular shape by quasi-helixes. Computers & Graphics 2014;38(1):392–8.

[42] Xin SQ, Wang W, Chen S, Zhao J, Shu Z. Intrinsic girth function for shape processing. ACM Transactions on Graphics 2015;35(3):1–14.